An active nanoporous Ni(Fe) OER electrocatalyst via selective dissolution of Cd in alkaline media

Jun-Hyuk Kim[a], Duck Hyun Youn[a,b], Kenta Kawashima[c], Jie Lin[a,d], Hyungseob Lim[c], C. Buddie Mullins[a,c,e,*]

[a] McKetta Department of Chemical Engineering, University of Texas at Austin, TX, 78712, United States
[b] Department of Chemical Engineering, Kangwon National University, Gangwondaehak-gil, Chuncheon, Gangwon-do, 24341, South Korea
[c] Department of Chemistry, University of Texas at Austin, TX 78712, United States
[d] Pen-Tung Sah Micro-Nano Science and Technology Institute, Xiamen University, Xiamen, Fujian, 361006, China
[e] Texas Materials Institute, University of Texas at Austin, TX 78712, United States

ARTICLE INFO

ABSTRACT

Although there has been a significant progress regarding electrocatalysts for the electrochemical oxygen evolution reaction, further breakthroughs are still required due to its sluggish 4-electron transfer mechanism. Ni is considered as a potential candidate for the oxygen evolution reaction (OER) in alkaline media in lieu of noble metals, however, the utility of Ni has been limited by the required and relatively high overpotentials. In this study, we fabricated a nanoporous Ni structure by selective and partial dissolution of Cd from a NiCd composite (without using hazardous acids or bases). The formation of nanoporous Ni greatly enhanced OER performance because of the increased number of catalytic sites. Furthermore, there was a promotional electronic effect on the electrocatalyst induced by Cd atoms under the Ni surface tuning the catalytic reactivity could be tuned. Additionally, Fe deposition on the porous Ni-Cd structure significantly raised the OER activity via a reduction in the overpotential from a value of $\eta = 382$ mV (before Fe deposition) to $\eta = 290$ mV (after Fe deposition) to achieve 10 mA cm^{-2}.

1. Introduction

Hydrogen and oxygen obtained from water splitting are very important as a power source with regard to the growing demand for renewable energy [1–3]. However, the oxygen evolution reaction (OER) process is a four-electron transfer reaction ($4OH^- \rightarrow O_2 + 2H_2O + 4e^-$ in an alkaline medium) limited by large overpotentials [4] and slow kinetics [5] so much research related to the OER regarding electrocatalysts, photocatalysts, or thermal decomposition pathways is currently underway. Among the various approaches for effective facilitation of the OER, employing electrocatalysts in alkaline electrolyte is considered one of the most viable solutions, especially considering the possibility of using alternative cheap earth-abundant catalysts [6] which can be applied as favorable oxygen electrocatalyts at the anode side [7]. Indeed, considering the cost of noble metals as OER electrocatalysts [8–11], there has been increasing interest in the application of non-noble metal based electrocatalysts (mostly 3d elements [7,12]). Among them, recent advances with Ni oxide have shown great improvement in OER activity and stability and nickel is abundant, cheap

and has high stability in alkaline solution. There have been many Ni-based investigations from oxide [13,14] to mixed metal oxide (Ni-Fe [15–17], Ni-V [18], Ni-Co [19]) in recent years. However, since the utility of Ni-oxide electrocatalysts has still been limited by the required high overpotentials, there have been many studies aimed at effective strategies for activity improvement; one promising approach is the fabrication/synthesis of nanoporous electrocatalysts [20]. Because of their unique intermetallic connections and high surface area, nanoporous structures are exceptionally attractive as OER electrocatalysts. Thus, several attempts to synthesize nanoporous structures or 3D architectures have been made via templating [21,22], solvothermal [23], nanocasting [24], electrospinning [25], and nitridation reaction [26] techniques. Additionally, a common approach to obtain nanoporous sponge materials is an electrochemical dissolution method [27]. With this method, the porous structure can be fabricated with ease by selective dissolution of an unstable element from a composite [20] without hazardous acids or bases. Furthermore, it can lead to geometric effects as well as promotional electronic effects by forming a different elemental composition in the surface and sub-surface layers [28] which

can alter the adsorption energy resulting in a tuning of the activity [29] since the OER consists of several elementary reaction steps involving adsorbates such as *O, *OH, and *OOH [30].

Here we describe our synthesis of a porous Ni structure with Cd (as a pore maker) which can be readily and effectively dissolved in an alkaline medium (pH 13–14) [31] for synergistic (geometry and electronic) electrocatalytic effects. Interestingly, nanoporous Ni electrocatalyst was clearly formed after Cd dissolution drastically enhancing OER performance compared to bulk Ni. Furthermore, a promotional electronic effect induced by Cd (at bulk) under Ni surface could promote the catalytic reactivity. Additionally, we readily deposited Fe on the porous Ni electrocatalyst using an electron-beam (e-beam). It basically proposes its empirical usage as a highly active nanoporous NiFe based electrocatalyst. The Fe evaporation boosted the OER activity from the overpotential of $\eta = 382$ mV (before Fe deposition) to $\eta = 290$ mV (at 10 mA cm^{-2}). Scanning electron microscopy (SEM), optical profilometry, X-ray diffraction (XRD), and electrochemical tests were conducted for the characterization of the nanoporous Ni electrocatalyst. X-ray photoemission spectroscopy (XPS) was employed to investigate potential electronic effects.

2. Experimental

2.1. Electrocatalyst fabrication

Polycrystalline titanium (1/4″ of diameter, 99.99% purity, and Kurt J. Lesker) was used as a substrate for the NiCd electrocatalyst. Details regarding preparations of the electrocatalyst can be found in reference [32] but a brief description of the synthetic procedure follows. Firstly, the Ti substrate was polished for ~30 min employing two different types of sandpaper (1500- and 2000-grit) and alumina powder having a particle size of 1 and 0.3 µm (CH instruments) in order to obtain a smooth surface. The polished Ti was then washed with distilled water three times while under sonication, and finally rinsed with distilled water in preparation for the deposition of Ni or NiCd.

The Ni or NiCd was electrodeposited on the prepared Ti under the modified conditions of Dougherty [33] at a constant cathodic current of 5 mA for 300 s without stirring. The solution for electrodeposition was prepared with water based mixing of NiSO$_4$ 6H$_2$O (9 mM) and (NH$_4$)$_2$SO$_4$ (25 mM) adjusting the pH to 3. For the NiCd electrocatalyst, the Cd precursor, 3CdSO$_4$ 8H$_2$O (0.5 mM), was also added to the deposition electrolyte. Before the deposition process, the prepared solution was bubbled and fully saturated with Ar gas. The electrodeposition was carried out employing a hanging meniscus rotating disk electrode (RDE) configuration [34,35] for precise surface area determination. After the deposition, the prepared samples were rinsed with distilled water thoroughly. In order to conduct a systematic investigation, we prepared three samples each of NiCd with increasing Cd ratios including 100:3, 100:5, 100:10 and 100:20 (Ni:Cd) and named the samples with the following convention: NiCd(I) for the initial NiCd prior to any processing and NiCd(A) for the material after Cd dissolution from the NiCd(I).

For the preparation of the NiCd(A) electrocatalysts, the potential was swept in the range of 1.35–1.55 V (vs. RHE) with a scan rate of 50 mV s^{-1} for 500 cycles under rotating of 1600 rpm (experimental details in Fig. S1). An e-beam evaporator was used for deposition of Fe for the synthesis of both NiFe and NiCd(A)Fe electrocatalyst materials (characterization details in Figs. S2–S4). The e-beam deposition rates were controlled by adjustment of the emission current with a rate of 0.2 Å/s for a thickness of 3 nm as measured by a quartz crystal microbalance (QCM). The main chamber pressure was maintained at a pressure of 1×10^{-7} during the evaporation (TEM images of evaporated Fe on C-coated Cu grid and Ni film represent in Fig. S4). The particle type NiCd catalyst with a molar ratio of 100:5 was prepared by a chemical reduction method. The stoichiometric amounts of NiSO$_4$·6H$_2$O and CdSO$_4$·8/3H$_2$O precursors were dissolved in 100 ml

of D.I water followed by addition of 50 ml of 0.1 M NaBH$_4$ solution under vigorous stirring. After 1 h of stirring, the solution was filtered, washed with excess amount of water and dried at 80 °C for 12 h in an oven. The NiCd(A)_P was prepared in the above manner for the NiCd (A).

2.2. Characterization

All the samples were quantitatively analyzed for Ni, Cd, and Fe by using an inductively coupled plasma mass spectrometry (ICP-MS). A three-electrode system was used for the evaluation of the electrochemical behavior with a potentiostat (CHI660D, CH instruments) consisting of a working electrode (catalyst), reference electrode (Ag/AgCl in sat. KCl, converted to RHE scale as shown in Fig. S5) and an auxiliary electrode (Pt mesh). Cyclic voltammetry (CV) was conducted in the voltage range 1.0–1.1 V vs. RHE with a scan rate of 10, 20, 50, and 100 mV s^{-1} in Ar fully purged 0.1 M NaOH electrolyte in order to estimate the electrochemical surface area (ECSA). The water oxidation reaction was evaluated by measuring an anodic current sweep using linear sweep voltammetry (LSV) in the voltage range between 1.0–1.9 V with a scan rate of 5 mV s^{-1}. All electrochemical data have been corrected with an i-R compensation (27 Ω) and obtained at room temperature under ambient pressure. The total metal loading of catalysts was identical for electrochemical test as shown in Tables S1–S2 and S4. The NiCd(A)_P was dispersed on a glassy carbon electrode (1/4″ of diameter) with 89.6 ml of D.I water, 10 ml of isopropanol, and 0.4 ml of Nafion solution (5%). The 30 µl of ink was dropped on the working electrode with the same metal loading of the NiCd(A) catalyst. The surface of the thin film was observed using scanning electron microscopy (SEM, FEI Quanta 650 SEM) without a noble metal coating. The accelerating voltage was 15 kV with 2 nA of current and a 10 mm working distance. The surface profile was measured using a non-contact optical profilometer (Wyko NT 9100, FOV 2.0 X). XPS spectra were recorded on a Kratos Axis Ultra DLD spectrometer using monochromatic Al Kα radiation (1486.6 eV) with 400 µm spot sizes of X-ray monochromator under 1×10^{-10} Torr for information on elemental composition and chemical bonding states of samples. All XPS energy data were calibrated with the C 1s electron peak (284.6 eV). The samples were structurally characterized by X-ray diffraction (XRD, Rigaku Ultima IV) equipped with CuKα radiation (λ = 1.54056 Å) using a fixed glancing incidence angle α = 1° at room temperature. Rietveld analyses were performed using the PANalytical X'pert highscore software (Philips, Netherlands). The microstructure of the catalytic film was investigated by using TEM (JEOL 2010F) with an electron gun operated at 200 KV.

3. Results and discussion

In order to identify the optimal compositions of Ni and Cd for creating active porous Ni electrocatalysts, the OER performance was measured with various ratio of Ni to Cd. Fig. 1 shows OER polarization curves for NiCd electrocatalysts as a function of Cd ratio (Ni:Cd = 100:3, 100:5, 100:10, and 100:20). The onset potential for OER shifted positively with an increasing ratio of Cd (Ni:Cd = 100:10 and 100:20). The Cd in the samples with the ratio of 100:10 and 100:20 may cover the active Ni sites while the samples with relatively low portion of Cd (100:3 and 100:5) required less overpotential and showed similar initial OER performance. All the samples have a significant activity enhancement after Cd dissolution, it is interesting to note that the electrocatalyst with Ni:Cd = 100:5 showed the best performance which could have optimal trade-off characteristics between pores and structural integrity. Thus, we decided to focus on the NiCd (100:5) material in this study of OER electrocatalysts.

Scanning electron microscopy (SEM) was used to examine the surface morphology of the samples. The microstructure of the NiCd(I) and NiCd(A) along with Ni films are shown via the SEM images shown in
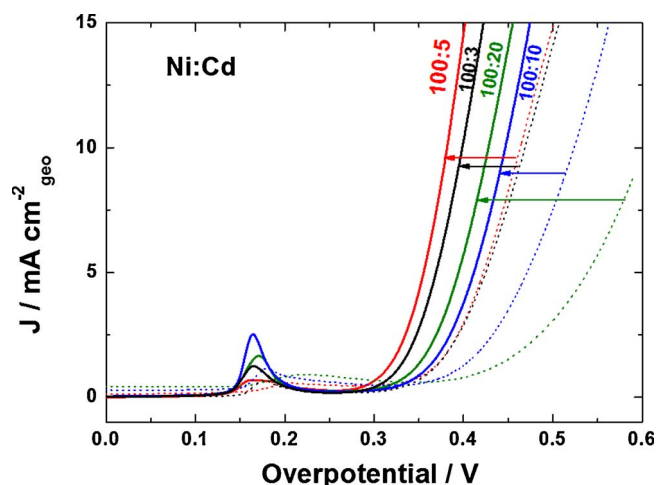
Fig. 1. OER polarization curve for NiCd electrocatalysts as a function of Cd ratio (Ni:Cd = 100:3, 100:5, 100:10, and 100:20). Dotted lines represent initial NiCd (before Cd dissolution). All the data was collected with the scan rate of 5 mV s^{-1} in Ar fully purged 0.1 M NaOH electrolyte.

Fig. 2a–d. Grain size was determined as roughly 100 nm for Ni, 250 nm for the NiCd(I) and the NiCd(A), respectively. The thickness of the films was estimated to be ~3 μm as shown in Fig. S6.
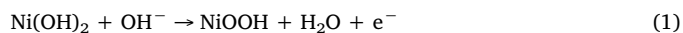
As shown in Fig. 2b, the SEM image of the NiCd(I) sample indicates that the substrate surface was completely covered by a Ni and Cd mixture. The formation of a porous structure of Ni began with electrochemical dissolution by removing surface exposed Cd atoms, for which Cd has a thermodynamically high solubility at high pH. [31] With this feature, selective dissolution of Cd was generated as shown in Fig. 2c and it remained Ni atoms onto the surface dominantly left Cd atoms into subsurface of the structure, which formed interconnected porous NiCd structure. The dissolution of Cd atoms also can be estimated by analysis of the EDS spectrum and quantitative elemental data (details in Figs. S7–S8). Fig. 2d shows the ratio of Ni:Cd in NiCd(I) and NiCd(A) was calculated with the relative weight percent of Ni as 100%. The relative Cd ratio drastically decreased from 35 ± 7 to 13 ± 5%, clearly showing selective dissolution of Cd. The roughness in the porous structure was also clearly observed via the optical profilometer

technique as shown in Fig. 2e–f. The surface roughness parameter (R_t) of the NiCd(A) sample showed more than a 5-fold increase compared to pure nickel [from 3.01 μm for Ni and 5.26 μm for NiCd(I) to 16.42 μm for NiCd(A)] due to the dissolution of surface Cd. The R_t of the NiFe catalyst (3.28 μm) is similar to that of the pure Ni catalyst (see Fig. S9).

In order to gain insight into the porous structure, XRD was used in the NiCd(I) and NiCd(A) as shown in Fig. 3, using a fixed grazing angle of incidence (GIXRD). Since the NiCd sample is a thin film it will only produce a weak diffraction signal, but a fixed angle mode instead of conventional θ/2θ scanning can enhance the signal by reducing the intense signal from the substrate. For more detailed structural analysis, we performed Rietveld refinement with the data from the NiCd sample. Metallic phases of Ni (cubic close-packed, JCPDS file no. 00-001-1258) and Cd (hexagonal close-packed, 01-085-1328) were observed in both of the NiCd(I) and NiCd(A), no other phases or amorphous components except for Ni and Cd are present in detectable quantities by the refinement. The obtained quantitative result suggests that the Cd ratio (%) decreased in the NiCd(A) sample to 97:3 from the initial NiCd(I) 84:16, which is in close agreement with the result from SEM analysis.

We next attempted to optimize the effectiveness of the porous Ni structure by depositing a small amount of Fe as explained in the last part of introduction section since Ni and Fe mixed oxyhydroxides are currently known as one of the most active OER catalysts in alkaline electrolyte [36] and there are several reports that the introduction of Fe can enhance the OER activity. [16,37,38]

The OER activity was evaluated electrochemically using rotating disk electrode (TF-RDE) measurements. The substrate Ti can be seen to be electrochemically inert toward the OER catalyst over the entire experimental potential range (Fig. S11). Polarization curves for the OER with the various samples are shown in Fig. 4a. An anodic current feature appears at a potential of ~1.39 V vs. RHE for both Ni and NiCd(A) and is consistent with Ni being oxidized to Ni(OH)$_2$ as described in a previous report: [39]

$$Ni(OH)_2 + OH^- \rightarrow NiOOH + H_2O + e^- \tag{1}$$

where reaction occurs in the potential range 1.38–1.40 V [37,40,41]. The OER activity for NiCd(A) (η = 382 mV at 10 mA cm^{-2}) was higher than that of pure Ni (η = 433 mV), primarily due to the enhanced surface area from the NiCd(A) porous structure. The NiFe electrocatalyst, which has highly optimal adsorption energies for OER intermediates which enhance the performance [16], showed the same trend
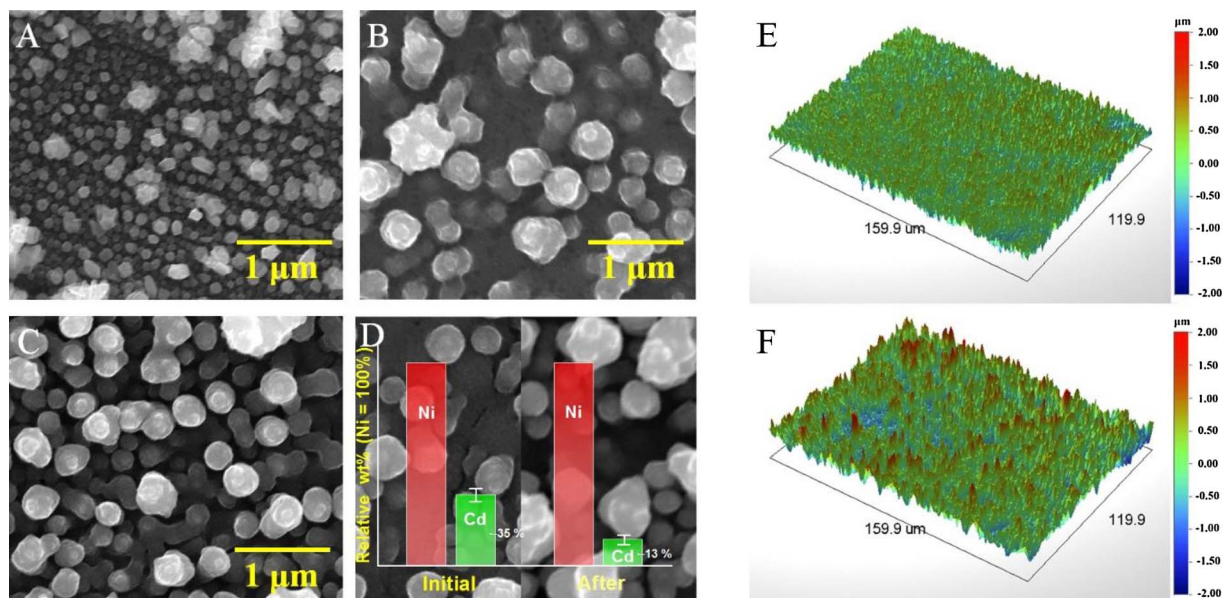

Fig. 2. Top-view SEM images of (a) Ni, (b) NiCd(I), and (c) NiCd(A). (d) Relative Ni and Cd composition ratio of NiCd(I) and NiCd(A) obtained from EDS. Surface profiles obtained using a 3D optical profilometer for (e) Ni and (f) NiCd(A). The NiCd(I) and NiCd(A) represent for the initial NiCd catalyst and the catalyst after Cd dissolution from the NiCd(I), respectively.
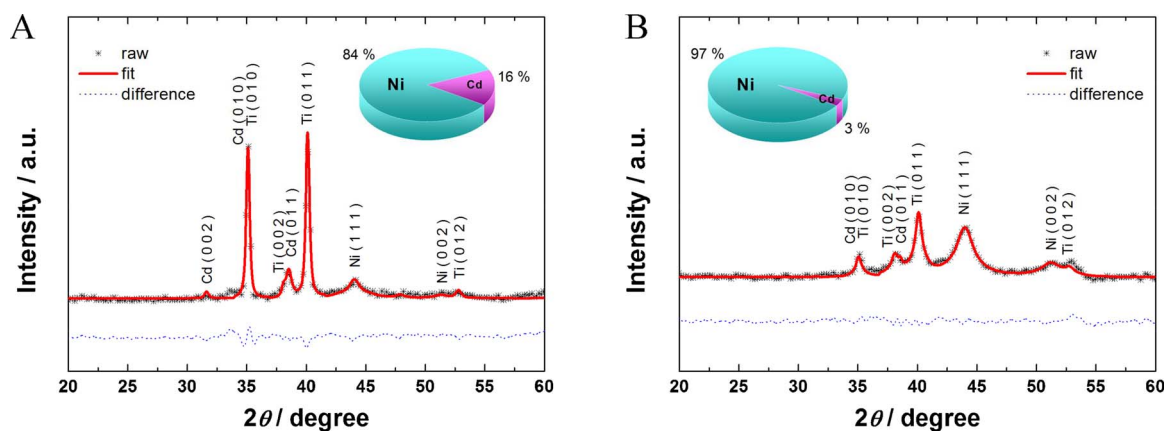
Fig. 3. The Rietveld refinement of the XRD pattern for (a) NiCd(I) and (b) NiCd(A). The blue line denotes the difference between the raw and the simulated profiles. The composition ratio of Ni and Cd phases in the same structure is described in insets (weight, %). (For interpretation of the references to colour in this figure legend, the reader is referred to the web version of this article.)

in this electrochemical study. The overpotential of the NiFe electrocatalyst (η = 337 mV) was drastically lower than both those for pure Ni (η = 415 mV) and even the porous Ni at the same current density (10 mA cm^{-2}). Interestingly, the most active OER catalyst was the NiCd(A)Fe (η = 290 mV) in which the overpotential for 10 mA cm^{-2} was shifted by 47 mV compared to the non-porous NiFe catalyst.

Fig. 4b. shows the Tafel slopes for the Ni, NiCd(A), NiFe, and NiCd(A)Fe electrocatalysts. A Tafel plot is known as one of the most effective indicator for the OER catalytic behavior of materials in terms of surface kinetics and elucidation of the reaction mechanism [38]. The smallest

Tafel slope of 38 mV dec^{-1} was achieved for the NiCd(A)Fe sample which implies the most favorable OER process on this sample. This value was better than that of the NiFe sample (51 mV dec^{-1}), and both values are consistent with NiFe (oxy)hydroxide electrocatalysts reported in the literature which vary between 25 and 60 mV dec^{-1} [38]. Tafel slopes were slightly lower in samples with no iron doping (59 mV dec^{-1} for the NiCd(A) and 75 mV dec^{-1} for the Ni. The improved kinetics is attributed to the increase in the number of active surface sites for the porous structure [42], which has been confirmed by ECSA.
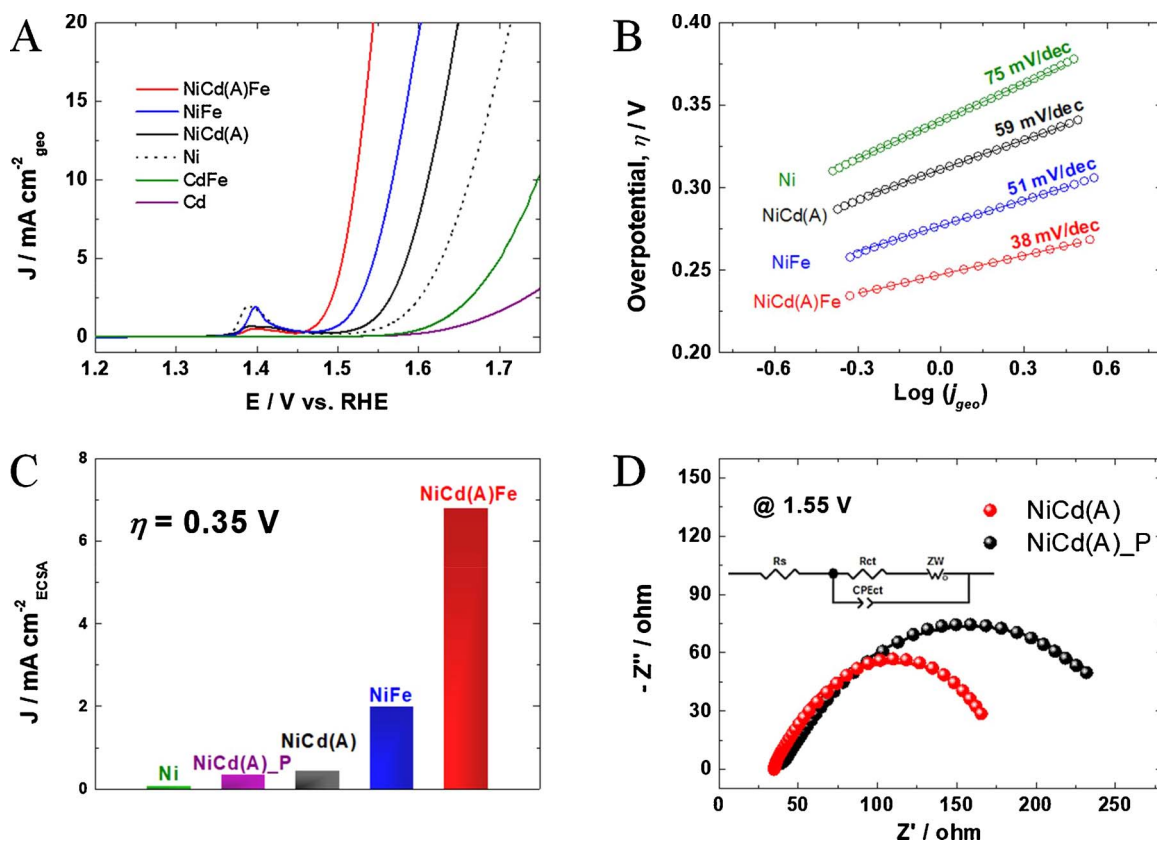

Fig. 4. Electrochemical test results of various catalysts based on Ni. (a) OER polarization curves, (b) Tafel plots, (c) specific activity (per ECSA) at η = 0.35 V for Ni, NiCd(A), and NiCd(A)Fe with NiFe, NiCd(A)_P [NiCd(A) particles], CdFe, and Cd for comparison. (d) Electrochemical impedance spectra of NiCd(A) prepared with different type of catalyst (film and particle). The atomic composition of elements in the catalysts: Ni (92%), Cd (8%) in the NiCd(A) and Ni (94%), Cd (6%) in the NiCd(A)_P and Ni (84%), Fe (16%) in the NiFe, and Ni (73%), Cd (9%), Fe (18%) in the NiCd(A)Fe (see Table S3). The NiCd(A) sample was conditioned by sweeping the potential in the range of 1.35–1.55 V (vs. RHE) with a scan rate of 50 mV s^{-1} for 500 cycles (see experimental section). All the data was collected in an Ar fully purged 0.1 M NaOH electrolyte.

The intrinsic activity of the samples can be reported based on actual surface area as well as geometric surface area. The ECSA measurements provide information regarding the actual surface for electrochemical reaction. In particular, the ECSA measurement is essential for porous or high roughness factor (RF) catalysts since surface imperfections contributes to the actual surface area being greater than the corresponding geometrical area [43]. Here, we measure the ECSA for each sample from the electrochemical double-layer capacitance of the catalytic surface [44,45] with a typical specific capacitance of $0.040 \, \mathrm{mF \, cm^{-2}}$ reported for a metal electrode in an aqueous NaOH solution [46] (estimation details in Fig. S12). The current densities of the samples employing ESCA determined surface areas at the overpotential of $\eta = 350 \, \mathrm{mV}$ are shown in Fig. 4c. The highest specific activity was observed with the NiCd(A)Fe sample ($6.79 \, \mathrm{mA \, cm^{-2}_{ECSA}}$), and the order followed the sequence: NiFe ($2.00 \, \mathrm{mA \, cm^{-2}_{ECSA}}$) > NiCd(A) ($0.46 \, \mathrm{mA \, cm^{-2}_{ECSA}}$) > NiCd(A)_P [NiCd(A) particles] ($0.36 \, \mathrm{mA \, cm^{-2}_{ECSA}}$) > Ni ($0.09 \, \mathrm{mA \, cm^{-2}_{ECSA}}$). The value for pure Ni is in good agreement with observations reported by Jaramillo et al. in which the specific current density of oxidized Ni at $\eta = 350 \, \mathrm{mV}$ is in the range of $0.07–0.17 \, \mathrm{mA \, cm^{-2}_{ECSA}}$ [45]. It is readily apparent that the intrinsic OER activity was improved in the porous structure from a metallic interconnection as well as larger surface area to electrolyte so that the mass transport was enhanced [42].

It is known that particular microstructures with a large density of grain boundaries can impact negatively on OER performance with a higher resistance [47]. This impact can be further studied with the techniques of electrochemical impedance spectroscopy (EIS) as shown in the Nyquist plots in Fig. 4d. The semicircle in the high-frequency region exhibits the charge transfer resistance (R_{ct}) from the bulk electrolyte to the catalyst surface, which is unaffected to the potential applied [21]. Metal interconnected porous NiCd(A) showed a lower value for R_{ct} in comparison with the NiCd(A) particles [NiCd(A)_P] (Table S5) resulting from an efficient pathway for electron transport in the porous structure providing the conductive channel [42].

Overall, the porous electrocatalyst showed an excellent intrinsic OER activity (based on both geometry and ECSA) and comparable stability (as shown in Fig. S13) compared to other samples and possibly a promotional electronic effect due to the formation of a Ni (surface) – Cd (bulk) structure via Cd dissolution at the top most layers. For this reason, we carried out further analysis for the NiCd(A) samples to understand their enhanced performance due to electronic structure changes.

XPS analysis was carried out in order to observe the electronic properties of Ni in the surface layers. Fig. 5 shows the result of the XPS analysis of Ni $2p_{3/2}$ for the Ni, NiCd(I), and NiCd(A) samples. An XPS deconvolution analysis revealed that both the Ni and NiCd(I) were mainly covered with oxygen species. According to Rubio-Zuazo's research, the information depth is $\sim 10 \, \mathrm{nm}$ (at 99% of detection) and

$\sim 14 \, \mathrm{nm}$ (at 99.8%) for a 1.5 keV photoelectron kinetic energy [48]. In this study, XPS signals might be detected from the surface also the sub-surface (mainly reflecting Ni^0) which might be attributed to the rough sample surface or the high take-off angle (90°) [49].

It was determined that the Ni^0 at $\sim 852 \, \mathrm{eV}$ contributed 31 and 22.5% of peak area percentages for the total Ni $2p_{3/2}$ signal for the pure Ni and NiCd(I) samples, respectively (Table S6). The peak at $\sim 855.80 \, \mathrm{eV}$ is associated with $Ni^{2+/3+}$ species corresponding to Ni $(OH)_2$ and/or γ-NiOOH since the peak position is not sensitive enough to set apart these two compounds from one another [50]. The peak in the higher binding energy region above 860 eV is thought to be correlated with satellites [50].

Since it is reported that co-deposition can give rise to a homogeneous distribution of elements throughout a thick film ($\sim 1 \, \mu m$) [51], the XPS results in our study indicate electron charge transfer from Ni might occur in Ni-Cd mixtures. Because the percentage of the oxidation state except for metallic Ni was differed as 69.0 and 77.5% for Ni and NiCd(I), respectively. In order to examine the charge transfer, the Cd 3d core spectrum was further studied (Fig. S14), however it was difficult to obtain meaningful information due to the similar chemical states of the metal and oxidized phases [52–55]. Since higher valent Ni species can be beneficial to greater catalytic OER activity [51] and the charge transfer is able to promote Ni into an oxidation state that can enhance OER performance, further study regarding clarification of the charge transfer should be undertaken.

The Ni $2p_{3/2}$ core spectrum in the NiCd(A) sample is represented in Fig. 5c. The chemical oxidation state of Ni was changed in the NiCd(A) compared to the NiCd(I), metallic Ni phase more reduced and the peak assigned to $Ni(OH)_2$ dominantly possessed at the NiCd(A) surface. This could be from the repetitive electrochemical cycling for the Cd dissolution process.

Fig. 6 gives the valence band XPS spectra for the Ni and NiCd(A) samples. The surface valence band photoemission spectrum was vertically aligned relative to the Fermi level ($E_F = 0$). Analysis of the valence band has received considerable attention in the literature since it represents information regarding the *d*-band center, which is a very general descriptor of the reactivity of a surface [56]. Although the main features in valence band region remained the same in the Ni and NiCd (A), the *d*-band center shifted upward relative to E_F in the NiCd(A) (3.91 eV) sample relative to that for the Ni (4.01 eV) sample. This higher binding energy of the *d*-band center can be attributed to the electronic interaction between neighboring Ni and Cd atoms and surface strain attributed to the different atomic radii of Ni (0.56–0.7 Å) and Cd (0.84–1.31 Å) atoms [57,58].

Koper and Calle-Vallejo et al. reported on the Sabatier-type volcano activity curve trend of OER on the basis of a HO* and HOO* adsorption energies on a Ni-based oxyhydroxide. [30] In their activity plot, NiOOH is located on the right leg (the weak binding side) and needs to be
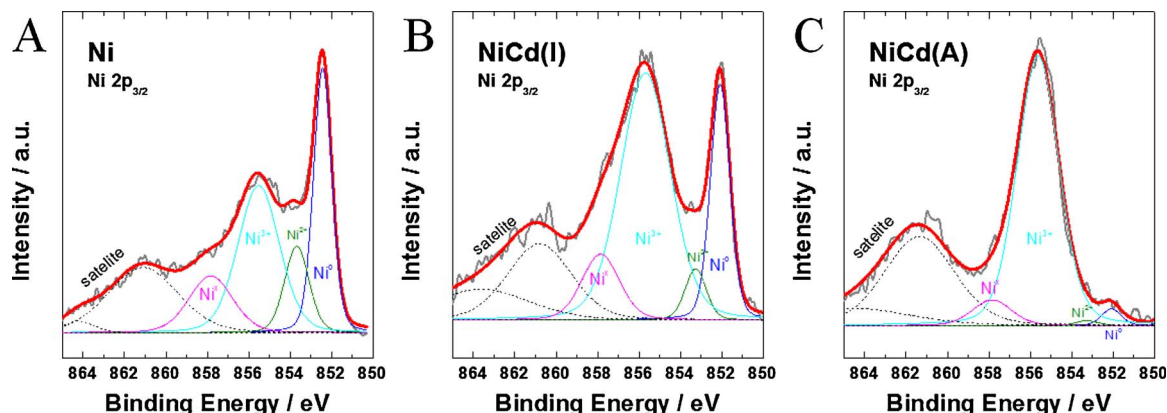

Fig. 5. XPS analysis of Ni $2p_{3/2}$ for (a) Ni, (b) NiCd(I), and (c) NiCd(A). Here, "Ni" refers to the catalyst before OER sweeps.
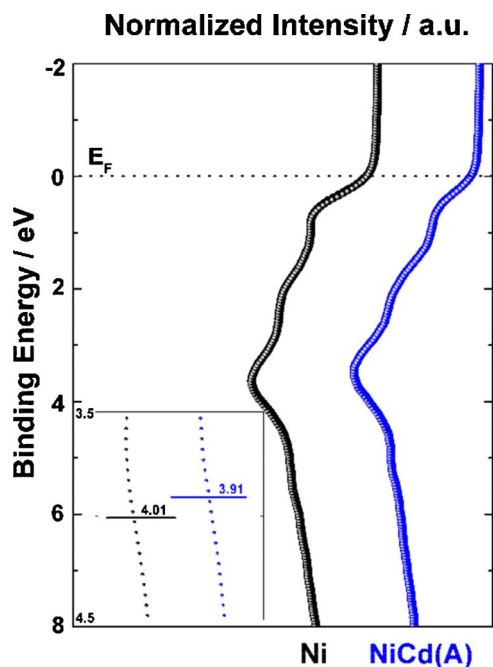
Normalized Intensity / a.u.

Fig. 6. (a) Valence band XPS spectra for the Ni and NiCd(A) samples. The Ni and NiCd(I) were electrodeposited (as described in the text) and two both samples underwent 500 cycles of CV (from 1.35 V–1.55 V at 50 mV) to create NiCd(A) and for fair comparison. Inset: magnified region from 3.5–4.5 eV in the vicinity of the *d*-band center. The binding energy was scanned over the range from 0 to 10 eV.

modified so that the bond strength to adsorbates is increased in order to reduce the OER overpotential [30]. Therefore, one of the strategies is to strengthen the bond with adsorbates for active surface Ni^{2+}/Ni^{3+} species than for pure NiOOH. Since it is known that a *d*-band center upshift can increase the bond strength to adsorbates [58,59], the electronic effect observed in this study may result in stronger surface bonds thereby favorably tuning OER activity.

4. Conclusions

In this work, a porous Ni structure was created via the selective dissolution of Cd for synergistic (geometry and electronic) effects. The nanoporous Ni electrocatalyst was characterized by SEM, XRD, and optical profilometry. Porosity could enhance the surface area drastically enhancing OER performance, moreover electronic effect derived from sub-surface Cd atoms could promote the activity. Finally, we deposited Fe atoms on the porous Ni nanostructured catalyst resulting in a marked enhancement of the OER performance (η = 290 mV at 10 mA cm^{-2}).

Acknowledgment

Appendix A. Supplementary data

Supplementary data associated with this article can be found, in the online version, at http://dx.doi.org/10.1016/j.apcatb.2017.11.053.

References

[1] T. Maiyalagan, K.A. Jarvis, S. Therese, P.J. Ferreira, A. Manthiram, Spinel-type lithium cobalt oxide as a bifunctional electrocatalyst for the oxygen evolution and oxygen reduction reactions, Nat. Commun. 5 (2014) 3949.

[2] K.L. Pickrahn, S.W. Park, Y. Gorlin, H.-B.-R. Lee, T.F. Jaramillo, S.F. Bent, Active MnOx electrocatalysts prepared by atomic layer deposition for oxygen evolution and oxygen reduction reactions, Adv. Energy Mater. 2 (2012) 1269.

[3] H. Ibrahim, A. Ilinca, J. Perron, Energy storage systems – characteristics and comparisons, Renew. Sustain. Energ. Rev. 12 (2008) 1221.

[4] S. Song, H. Zhang, X. Ma, Z. Shao, R.T. Baker, B. Yi, Electrochemical investigation of electrocatalysts for the oxygen evolution reaction in PEM water electrolyzers, Int. J. Hydrogen Energy 33 (2008) 4955.

[5] J. Rossmeisl, A. Logadottir, J.K. Nørskov, Electrolysis of water on (Oxidized) metal surfaces, Chem. Phys. 319 (2005) 178.

[6] J. Suntivich, K.J. May, H.A. Gasteiger, J.B. Goodenough, Y. Shao-Horn, A perovskite oxide optimized for oxygen evolution catalysis from molecular orbital principles, Science 334 (2011) 1383.

[7] E. Fabbri, A. Habereder, K. Waltar, R. Kotz, T.J. Schmidt, Developments and perspectives of oxide-based catalysts for the oxygen evolution reaction, Catal. Sci. Technol. 4 (2014) 3800.

[8] T. Reier, M. Oezaslan, P. Strasser, Electrocatalytic oxygen evolution reaction (OER) on Ru Ir, and Pt catalysts: a comparative study of nanoparticles and bulk materials, ACS Catal. 2 (2012) 1765.

[9] N. Danilovic, R. Subbaraman, K.C. Chang, S.H. Chang, Y. Kang, J. Snyder, A.P. Paulikas, D. Strmcnik, Y.T. Kim, D. Myers, V.R. Stamenkovic, N.M. Markovic, Using surface segregation to design stable Ru-Ir oxides for the oxygen evolution reaction in acidic environments, Angew. Chem. Int. Ed. 53 (2014) 14016.

[10] Y. Lee, J. Suntivich, K.J. May, E.E. Perry, Y. Shao-Horn, Synthesis and activities of rutile IrO$_2$ and RuO$_2$ nanoparticles for oxygen evolution in acid and alkaline solutions, J. Phys. Chem. Lett. 3 (2012) 399.

[11] W. Hu, Y. Wang, X. Hu, Y. Zhou, S. Chen, Three-dimensional ordered macroporous IrO$_2$ as electrocatalyst for oxygen evolution reaction in acidic medium, J. Mater. Chem. 22 (2012) 6010.

[12] R. Subbaraman, D. Tripkovic, K.-C. Chang, D. Strmcnik, A.P. Paulikas, P. Hirunsit, M. Chan, J. Greeley, V. Stamenkovic, N.M. Markovic, Trends in activity for the water electrolyser reactions on 3d M(Ni,Co,Fe,Mn) hydr(oxy)oxide catalysts, Nat. Mater. 11 (2012) 550.

[13] L. Wang, H. Chen, Q. Daniel, L. Duan, B. Philippe, Y. Yang, H. Rensmo, L. Sun, Promoting the water oxidation catalysis by synergistic interactions between Ni (OH)$_2$ and carbon nanotubes, Adv. Energy Mater. 6 (2016) 1600516.

[14] O. Mabayoje, A. Shoola, B.R. Wygant, C.B. Mullins, The role of anions in metal chalcogenide oxygen evolution catalysis: electrodeposited thin films of nickel sulfide as pre-catalysts, ACS Energy Lett. 1 (2016) 195.

[15] M. Gong, Y. Li, H. Wang, Y. Liang, J.Z. Wu, J. Zhou, J. Wang, T. Regier, F. Wei, H. Dai, An advanced Ni-Fe layered double hydroxide electrocatalyst for water oxidation, J. Am. Chem. Soc. 135 (2013) 8452.

[16] M. Gong, H. Dai, A mini review of niFe-based materials as highly active oxygen evolution reaction electrocatalysts, Nano Res. 8 (2015) 23.

[17] J.R. Swierk, S. Klaus, L. Trotochaud, A.T. Bell, T.D. Tilley, Electrochemical study of the energetics of the oxygen evolution reaction at nickel iron (Oxy)Hydroxide catalysts, J. Phys. Chem. C 119 (2015) 19022.

[18] K. Fan, H. Chen, Y. Ji, H. Huang, P.M. Claesson, Q. Daniel, B. Philippe, H. Rensmo, F. Li, Y. Luo, L. Sun, Nickel–vanadium monolayer double hydroxide for efficient electrochemical water oxidation, Nat. Commun. 7 (2016) 11981.

[19] C. Bocca, A. Barbucci, M. Delucchi, G. Cerisola, Nickel–cobalt oxide-coated electrodes: influence of the preparation technique on oxygen evolution reaction (OER) in an alkaline solution, Int. J. Hydrogen Energy 24 (1999) 21.

[20] C. Baldizzone, L. Gan, N. Hodnik, G.P. Keeley, A. Kostka, M. Heggen, P. Strasser, K.J.J. Mayrhofer, Stability of dealloyed porous Pt/Ni nanoparticles, ACS Catal. 5 (2015) 5000.

[21] J. Qi, W. Zhang, R. Xiang, K. Liu, H.-Y. Wang, M. Chen, Y. Han, R. Cao, Porous nickel-iron oxide as a highly efficient electrocatalyst for oxygen evolution reaction, Adv. Sci. 2 (2015) 1500199.

[22] X.Y. Yu, Y. Feng, B.Y. Guan, X.W. Lou, U. Paik, Carbon coated porous nickel phosphides nanoplates for highly efficient oxygen evolution reaction, Energy Environ. Sci. 9 (2016) 1246.

[23] M. Gao, W. Sheng, Z. Zhuang, Q. Fang, S. Gu, J. Jiang, Y. Yan, Efficient water oxidation using nanostructured α-nickel-hydroxide as an electrocatalyst, J. Am. Chem. Soc. 136 (2014) 7077.

[24] C. Xiao, X. Lu, C. Zhao, Unusual synergistic effects upon incorporation of Fe and/or Ni into mesoporous Co$_3$O$_4$ for enhanced oxygen evolution, Chem. Commun. 50 (2014) 10122.

[25] A. Vignesh, M. Prabu, S. Shanmugam, Porous LaCo$_{1?x}$Ni$_x$O$_{3-δ}$ nanostructures as an efficient electrocatalyst for water oxidation and for a zinc–air battery, ACS Appl. Mater. Inter. 8 (2016) 6019.

[26] Y. Wang, C. Xie, D. Liu, X. Huang, J. Huo, S. Wang, Nanoparticle-stacked porous nickel–iron nitride nanosheet: a highly efficient bifunctional electrocatalyst for overall water splitting, ACS Appl. Mater. Inter. 8 (2016) 18652.

[27] J. Erlebacher, M.J. Aziz, A. Karma, N. Dimitrov, K. Sieradzki, Evolution of nanoporosity in dealloying, Nature 410 (2001) 450.

[28] D. Wang, H.L. Xin, R. Hovden, H. Wang, Y. Yu, D.A. Muller, F.J. DiSalvo, H.D. Abruña, Structurally ordered intermetallic platinum-cobalt core-shell nanoparticles with enhanced activity and stability as oxygen reduction electrocatalysts, Nat. Mater. 12 (2013) 81.

[29] J.W.D. Ng, M. García-Melchor, M. Bajdich, P. Chakthranont, C. Kirk, A. Vojvodic, T.F. Jaramillo, Gold-supported cerium-doped NiO$_x$ catalysts for water oxidation, Nat. Energy 1 (2016) 16053.

[30] O. Diaz-Morales, I. Ledezma-Yanez, M.T.M. Koper, F. Calle-Vallejo, Guidelines for

the rational design of Ni-based double hydroxide electrocatalysts for the oxygen evolution reaction, ACS Catal. 5 (2015) 5380.

[31] D. Tromans, Pitting behavior of passivated cadmium monocrystals, J. Electrochem. Soc. 156 (2009) C367.

[32] J.-H. Kim, H. Woo, J. Choi, H.-W. Jung, Y.-T. Kim, CO_2 electroreduction on Au/TiC: enhanced activity due to metal-support interaction, ACS Catal. 7 (2017) 2101.

[33] M.D. Merrill, R.C. Dougherty, Metal oxide catalysts for the evolution of O_2 from H_2O, J. Phys. Chem. C 112 (2008) 3655.

[34] M.D. Maciá, J.M. Campiña, E. Herrero, J.M. Feliu, On the kinetics of oxygen reduction on platinum stepped surfaces in acidic media, J. Electroanal. Chem. 564 (2004) 141.

[35] B.D. Cahan, H.M. Villullas, The hanging meniscus rotating-disk (HMRD), J. Electroanal. Chem. 307 (1991) 263.

[36] D. Friebel, M.W. Louie, M. Bajdich, K.E. Sanwald, Y. Cai, A.M. Wise, M.-J. Cheng, D. Sokaras, T.-C. Weng, R. Alonso-Mori, R.C. Davis, J.R. Bargar, J.K. Nørskov, A. Nilsson, A.T. Bell, Identification of highly active fe sites in (Ni,Fe)OOH for electrocatalytic water splitting, J. Am. Chem. Soc. 137 (2015) 1305.

[37] T.T.H. Hoang, A.A. Gewirth, High activity oxygen evolution reaction catalysts from additive-controlled electrodeposited Ni and NiFe films, ACS Catal. 6 (2016) 1159.

[38] F. Dionigi, P. Strasser, NiFe-based (Oxy)hydroxide catalysts for oxygen evolution reaction in non-acidic electrolytes, Adv. Energy Mater. 6 (2016) 1600621.

[39] X. Li, F.C. Walsh, D. Pletcher, Nickel based electrocatalysts for oxygen evolution in high current density in alkaline water electrolysers, Phys. Chem. Chem. Phys. 13 (2011) 1162.

[40] P. Oliva, J. Leonardi, J.F. Laurent, C. Delmas, J.J. Braconnier, M. Figlarz, F. Fievet, A.D. Guibert, Review of the structure and the electrochemistry of nickel hydroxides and oxy-Hydroxides, J. Power Sources 8 (1982) 229.

[41] L. Trotochaud, J.K. Ranney, K.N. Williams, S.W. Boettcher, Solution-cast metal oxide thin film electrocatalysts for oxygen evolution, J. Am. Chem. Soc. 134 (2012) 17253.

[42] Z. Wang, J. Li, X. Tian, X. Wang, Y. Yu, K.A. Owusu, L. He, L. Mai, Porous nickel-iron selenide nanosheets as highly efficient electrocatalysts for oxygen evolution reaction, ACS Appl. Mater. Inter. 8 (2016) 19386.

[43] S. Lowell, J.E. Shields, Powder surface area and porosity, Powder Surface Area and Porosity, Springer, Netherlands: Dordrecht, 1984, pp. 3–6.

[44] S. Trasatti, O.A. Petrii, Real surface area measurements in electrochemistry, J. Electroanal. Chem. 327 (1992) 353.

[45] C.C.L. McCrory, S.H. Jung, J.C. Peters, T.F. Jaramillo, Benchmarking heterogeneous

[46] electrocatalysts for the oxygen evolution reaction, J. Am. Chem. Soc. 135 (2013) 16977.

[46] S. Jung, C.C.L. McCrory, I.M. Ferrer, J.C. Peters, T.F. Jaramillo, Benchmarking nanoparticulate metal oxide electrocatalysts for the alkaline water oxidation reaction, J. Mater. Chem. A 4 (2016) 3068.

[47] W. Hu, S. Chen, Q. Xia, IrO_2/Nb-TiO_2 electrocatalyst for oxygen evolution reaction in acidic medium, Int. J. Hydrogen Energy 39 (2014) 6967.

[48] J. Rubio-Zuazo, G.R. Castro, Information depth determination for hard X-ray photoelectron spectroscopy up to 15 keV photoelectron kinetic energy, Surf. Interface Anal. 40 (2008) 1438.

[49] V.A. Bondzie, P. Kleban, D.J. Dwyer, XPS identification of the chemical state of subsurface oxygen in the O/Pd(110) system, Surf. Sci. 347 (1996) 319.

[50] H. Ali-Löytty, M.W. Louie, M.R. Singh, L. Li, H.G. Sanchez Casalongue, H. Ogasawara, E.J. Crumlin, Z. Liu, A.T. Bell, A. Nilsson, D. Friebel, Ambient-pressure XPS study of a Ni-Fe electrocatalyst for the oxygen evolution reaction, J. Phys. Chem. C 120 (2016) 2247.

[51] N. Li, D.K. Bediako, R.G. Hadt, D. Hayes, T.J. Kempa, F. Von Cube, D.C. Bell, L.X. Chen, D.G. Nocera, Influence of iron doping on tetravalent nickel content in catalytic oxygen evolving films, Proc. Natl. Acad. Sci. U. S. A. 114 (2017) 1486.

[52] V. Di Castro, G. Polzonetti, G. Contini, XPS study of the oxidation of a Cu-Cd thin film, Surf. Sci. 251 (1991) 814.

[53] S. Ciampi, V. Di Castro, C. Furlani, G. Polzonetti, Cadmium oxidation in different environments: an XPS study, J. Electron. Spectrosc. Relat. Phenom. 60 (1992) 375.

[54] D. Barreca, Nanostructured cadmium sulfide thin films by XPS, Surf. Sci. Spectra 9 (2002) 46.

[55] J.F. Moulder, W.F. Stickle, P.E. Sobol, K.D. Bomben, Handbook of x ray photoelectron spectroscopy, A Reference Book of Standard Spectra for Identification and Interpretation of XPS Data, Physical Electronics inc., 1992.

[56] F. Abild-Pedersen, J. Greeley, J.K. Norskov, Understanding the effect of steps strain, poisons, and alloying: methane activation on Ni surfaces, Catal. Lett. 105 (2005) 9.

[57] R.D. Shannon, C.T. Prewitt, Effective ionic radii in oxides and fluorides, Acta Crystallogr. Sect. B: Struct. Sci. B25 (1969) 925.

[58] M. Mavrikakis, B. Hammer, J.K. Norskov, Effect of strain on the reactivity of metal surfaces, Phys. Rev. Lett. 81 (1998) 2819.

[59] J.-H. Kim, S. Chang, Y.-T. Kim, Compressive strain as the main origin of enhanced oxygen reduction reaction activity for Pt electrocatalysts on chromium-doped titania support, Appl. Catal. B: Environ. 158 (2014) 112.